PLOS ONE

Differential effects of aquaporin-4 channel inhibition on BOLD fMRI and diffusion fMRI responses in mouse visual cortex

Yuji Komaki [ID], Clement Debacker [ID], Boucif Djemai, Luisa Ciobanu, Tomokazu Tsurugizawa [ID], Denis Le Bihan [ID]*

NeuroSpin/Joliot, CEA-Saclay Center, Gif-sur-Yvette, France

* denis.lebihan@gmail.com

Abstract

The contribution of astrocytes to the BOLD fMRI and DfMRI responses in visual cortex of mice following visual stimulation was investigated using TGN-020, an aquaporin 4 (AQP4) channel blocker, acting as an astrocyte function perturbator. Under TGN-020 injection the amplitude of the BOLD fMRI response became significantly higher. In contrast no significant changes in the DfMRI responses and the electrophysiological responses were observed. Those results further confirm the implications of astrocytes in the neurovascular coupling mechanism underlying BOLD fMRI, but not in the DfMRI responses which remained unsensitive to astrocyte function perturbation.

Introduction

Diffusion functional MRI (DfMRI) has been proposed as an alternative to blood oxygenation level dependent (BOLD) fMRI to monitor neural activity noninvasively [1]. Several studies have demonstrated that the DfMRI and BOLD fMRI responses to a variety of stimuli differed qualitatively and quantitatively (ie amplitudes and time courses of responses) [1–5] suggesting that mechanisms underlying BOLD and diffusion fMRI must be different, although this view has been controversial [6,7]. While BOLD fMRI relies on the indirect neurovascular coupling mechanism [8,9] the current hypothetical mechanism of DfMRI is thought to be related to the neural activation triggered cell swelling, for which there is a large body of evidence [10,11]. Beside the established fact that water diffusion as monitored with MRI decreases in tissues undergoing cell swelling in pathological, extraphysiological and physiological conditions [12–16] several preclinical studies relying on pharmacological challenges interfering with neurovascular coupling or cell swelling have confirmed that (1) the DfMRI and BOLD fMRI responses could be decoupled, confirming their differential mechanisms; (2) the DfMRI response is not dependent on neurovascular coupling, but, instead, sensitive to underlying neural swelling status [17–19] and (3) the DfMRI response follows neural activity status closely and more accurately than BOLD fMRI, especially under anesthetic or vasoactive drug conditions [17,20].

To further uncover the differences between DfMRI and BOLD fMRI mechanisms we investigated the contribution of astrocytes to both responses. Astrocytes have been shown to play a major role in the neurovascular coupling mechanism [21]. Interfering with astrocyte function should, thus, impact BOLD fMRI responses, but not necessarily neural responses which have been shown to persist unaltered after neurovascular coupling inhibition [19]. Hence, DfMRI responses should remain relatively independent from astrocyte activity if they originate directly from neurons. To test this hypothesis, we have used an aquaporin-4 channel blocker (2-(nicotinamide)-1,3,4-thia- diazole, TGN-020) [22]. In the brain aquaporin-4 (AQP) channels are exquisitely expressed on astrocytes cell membranes mainly at the astrocyte end-feet surrounding vessels in the perivascular spaces, regulating water flow between blood and brain [23] and, in turn, the astrocyte volume and cerebral blood flow (CBF) [24]. To verify that neuronal activity remained unchanged under AQP4 channel inhibition, we recorded local field potentials (LFP), which reflect local synaptic activity [25]. LFPs are correlated with BOLD fMRI signal responses in normal conditions compared to multiunit activity (MUA) [26] and we have previously shown that LFPs are also well correlated with DfMRI responses [17,20].

Material and methods

Animals

The study was performed on 34 adult mice (20-28g, C57BL/6J, male, Charles River laboratories, Lyon, France): 9 in each of the saline and the TGN-020 group in the MRI study; 8 in each of the saline and the TGN-020 group in electrophysiology study. Mice were housed in groups of six under a 12-hour light/dark cycle, with access to food and water *ad libitum*.

All animal experimental procedures were performed in accordance with the EU Directive 2010/63/EU for care and use of laboratory animals and approved by the Comité d'Ethique en Expérimentation Animale (CETEA) de la Direction des Sciences du Vivant (DSV) du Commissariat à l'Energie Atomique et aux Energies Alternatives (approval number: APAFIS#8472-2017010915542l22 v2).

Functional MRI acquisitions

MRI acquisitions were performed using a 17.2 Tesla MRI system (Bruker BioSpin, Etlingen, Germany) with a 25mm quadrature birdcage coil (RAPID Biomedical GmbH, Rimpar, Germany). The mice were anesthetized with isoflurane (1–1.5% in medical air containing 30% O_2) and placed inside the magnet in a dedicated animal bed. The respiratory cycle and body temperature were monitored during scanning (model 1025, SA Instruments, NY, USA). The body temperature was maintained at 37 ˚C by means of circulating hot water. An optical fiber for light stimulation was placed in front of the right eye of the mouse. After completing the animal set-up, the anesthesia was switched from isoflurane to medetomidine (s.c. 0.1 mg/kg bolus, 0.2 mg/kg/h continuous infusion, Orion Pharma, Espoo, Finland). Acquisition of functional MRI data started 30 minutes after the administration of the medetomidine bolus.

High resolution anatomical images of the whole brain were acquired using a Rapid Acquisition with Relaxation Enhancement (RARE) sequence with the following parameters: effective echo time (eTE) = 23 ms, repetition time (TR) = 2000 ms, RARE factor = 8, number of averages = 4, spatial resolution = 75 x 75 x 500 $(\mu m)^3$, number of slices = 21.

Functional BOLD and diffusion fMRI acquisitions were performed using a double spin echo echo-planar imaging (SE-EPI) sequence to mitigate the effects of eddy currents and background magnetic field gradients: TE = 24.5 ms, TR = 2000ms, number of averages = 1, spatial resolution = 200 x 200 x 1000 $(\mu m)^3$, number of slices = 9; b-value =, [0 (BOLD equivalent), 1000, 1800 s/mm^2], number of repetitions = 180.

The visual stimulus consisted in six blocks of a blue light (4μW, 20s, 2Hz, 10ms pulse duration) alternating with darkness rest periods (40s) using a light emitting diode (LED) and Arduino programming board (ArduinoCham, Switzerland). The Arduino programming board synchronized the trigger from the Bruker scanner during the fMRI scanning. BOLD fMRI data were acquired twice, DfMRI three times with b = 1000, and six times with b = 1800 in each session (before and after TGN-020 administration). TGN-020 (200 mg/kg i.p., Merck KGaA, Darmstadt, Germany), an AQP4 inhibitor [22], was administrated after an initial set of baseline BOLD fMRI and DfMRI measurements. Functional data were collected again after 15 minutes from TGN-020 administration. TGN-020 was administered to a group of nine mice, while the other nine (control group) received a saline injection.

MRI data analysis

As previously described [27], SPM12 software (Welcome Trust Center for Neuroimaging, UK) was used for statistical calculation of brain activity maps. Image processing, consisting of slice timing correction, motion correction (the effect of residual motion during scan was further regressed out), normalization of brain coordinates, and smoothing (Gaussian kernel with FWHM of 0.6 mm), was performed for all fMRI data before statistical analysis. Statistical t-maps were calculated using a generalized linear model. Activation was detected using a statistical threshold of $p < 0.05$ (false discovery rate (FDR) corrected for multiple comparisons). Regions of interest (ROIs) of primary visual cortex (V1) for the time course analysis were defined anatomically using the Allen Mouse Brain Atlas [28,29]. Signal responses before and after TGN-020 administration were compared using a paired t-test ($p<0.05$ FDR corrected) after correction for temporal drifts using a high-pass filter of 1/120 [Hz]. Signals within scans (6 blocks) and between sessions (2 times BOLD fMRI, 3 times b = 1000, and 6 times b = 1800 in each session) were averaged out. The Apparent Diffusion Coefficient (ADC) (in mm²/s) was further obtained at each time point using the following equation:

$$ADC = \frac{\ln(S_0/S_{1800})}{1800}$$

where S_0 and S_{1800} are signal intensities obtained for b = 0 and 1800 s/mm², respectively. The signal change was expressed as percentage with the average value at rest taken as 100%. Time courses before and after TGN-020 administration were compared using paired t-tests.

Electrophysiological recordings

Electrophysiological recordings were performed separately, outside the MRI bore. The animals, first anesthetized with 1.5% isoflurane, were placed in a stereotaxic frame (David Kopf Instruments, CA). The body temperature was maintained at 37˚C using a heating pad (DC temperature controller; FHC Inc., Bowdoin, ME, USA). The skull was exposed and multiple holes (1 mm diameter) were made with a dental drill for insertion of micro-electrodes. The multiple tungsten microelectrodes (< 1.0 MΩ, 1 μm tip and 0.127-mm shaft diameter, Alpha Omega Engineering, Nazareth, Israel) were positioned on the left visual cortex (AP -3.5 mm, ML -2.2 mm, DV -1.5 mm from the Bregma). After surgery, the anesthesia was switched from isoflurane to medetomidine (s.c. 0.1 mg/kg bolus, 0.2 mg/kg/h continuous infusion, Orion Pharma, Espoo, Finland) as in the fMRI protocol. Electrodes were connected to a differential AC amplifier Model 1700 (AM systems, Sequim, WA, USA), via a Model 1700 head stage (AM systems, Sequim, WA, USA). The electrophysiology signals were acquired at 10 kHz sampling rate using dedicated data acquisition software (Power Lab, AD Instruments, Dunedin, New Zealand). The reference electrode was positioned on the scalp. The visual stimulation

paradigm was the same as for fMRI, with six blocks of alternating blue light stimulation (20s, 2Hz, 10ms pulse duration) and rest (40s) periods in a dark room, under the four conditions (pre and post saline or TGN-020 injection).

Electrophysiological analysis

The raw electrophysiological signals were frequency-filtered at 100 Hz for LFP [30]. The filtered electrophysiological signals were squared and averaged at each time point to calculate LFP power after applying a moving average filter with a 0.5 s window width. In addition, raw signals were bandpass-filtered between 300 and 1000 Hz to investigate high-frequency spiking activity (defined as a signal exceeding the baseline mean + 2 standard deviations [31]). The AUC during the stimulation period (10–30 s) was compared with the pre-stimulation period (0–10 s). The peak amplitude was defined as the maximum value during stimulation.

Results

Electrophysiology

LFP amplitude increased in V1 upon 2Hz blue light stimulation (Fig 1a and 1b). There was no difference in the area under the curve (AUC) and the peak amplitude of LFPs and high-frequency spiking activity (S1 Fig) responses after saline or TGN-020 administration (p<0.05) (Fig 1c and 1d) confirming that TGN-020 has no detectable effect on neuronal responses in V1.

BOLD fMRI

BOLD activation maps (b = 0 s/mm^2) are shown in Fig 2a. BOLD fMRI responses in V1 were readily observed following blue light stimulation, (as well as in superior colliculus, SC, and lateral geniculate nucleus, LGN). The time course of the BOLD fMRI signals in V1 are shown in Fig 3a. While the overall time course of the BOLD fMRI responses was not different after saline or TGN-020 injection (Figs 3a and 4), their amplitudes were significantly higher (p<0.05) under TGN-020 than under saline.

Diffusion fMRI

The DfMRI responses (b = 1000 and b = 1800s/mm^2) were also clearly observed in V1 (as well as in SC and LGN), but with a slightly smaller spatial extent than with BOLD fMRI (Fig 2b and 2c). The amplitudes of the DfMRI responses in V1 were slightly higher than BOLD fMRI responses before saline or TGN-020 injection (Fig 3b and 3c). The amplitudes remained unchanged (p<0.05) after administration of TGN-020 or saline (Figs 3b, 3c and 4). The amplitude of the b1800 DfMRI response was slightly higher than the b1000 DfMRI response, corresponding to the water diffusion decrease observed upon visual stimulation, as reflected in the ADC time courses computed from b = 0 and b = 1800 s/mm^2 (Fig 3d). However, the ADC change was not significantly different between saline and TGN-020 injected groups (p < 0.05) (Fig 4). The mean ADC baseline value (before stimulation) was not significantly different (p<0.05) before and after injection of saline (0.62 and 0.61 10^{-3} mm^2/s, respectively) and before and after injection of TGN-020 (0.67 and 0.71 10^{-3} mm^2/s, respectively).

Discussion

BOLD fMRI has been widely used in research and clinical practice to investigate brain function noninvasively. BOLD contrast results from the magnetic susceptibility balance between oxy- and deoxy-hemoglobin in circulating erythrocytes [32] which depends on the tissue
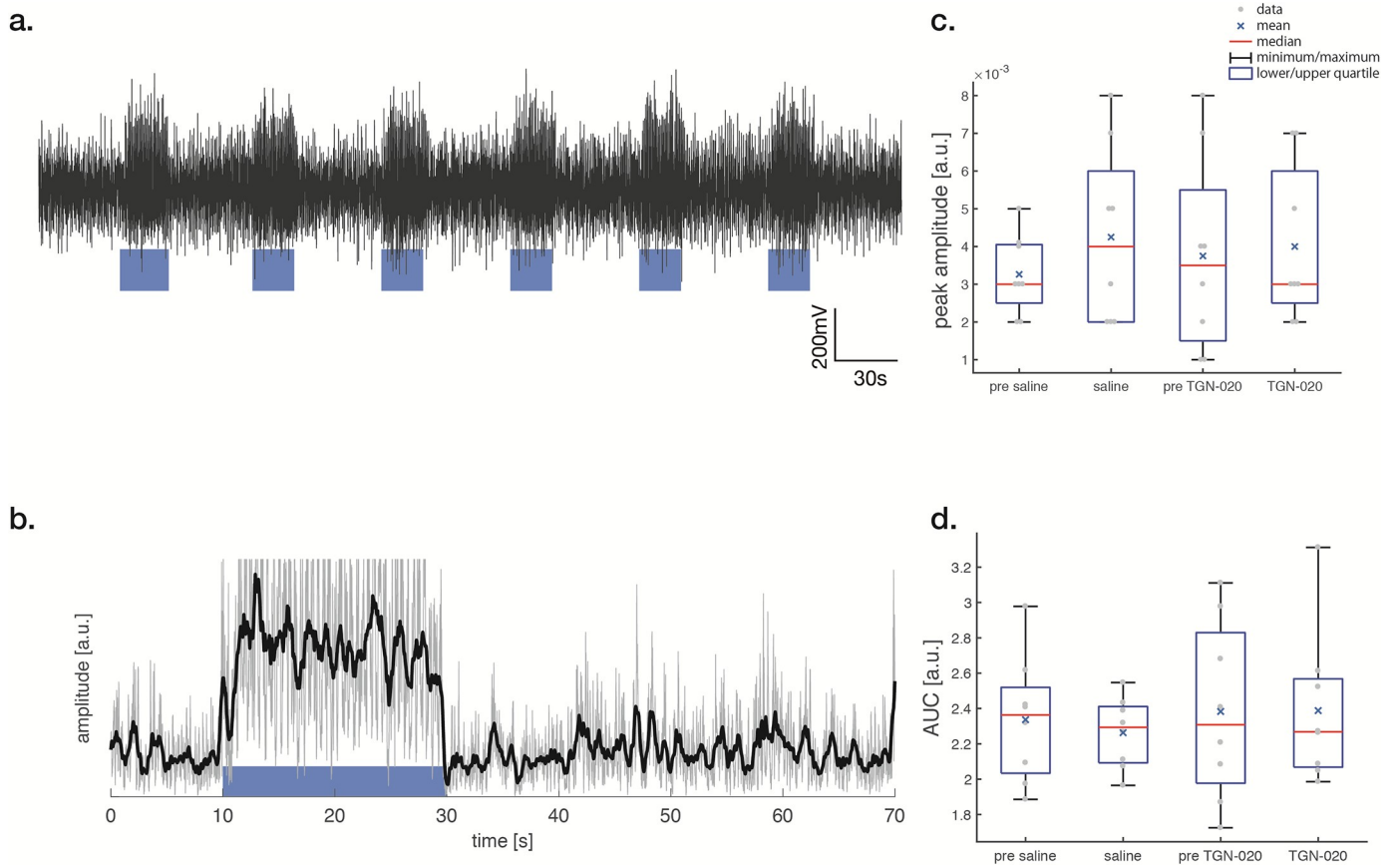
Fig 1. LFPs—Local Field Potentials (LFP) in V1 under blue light stimulation (a). The visual stimulus was applied between 10 and 30 seconds (a, blue block). The 100 Hz frequency filtered signal was squared and averaged at each time point (b, gray line). LFP power is obtained by applying a moving average filter of 0.5 s window width (b black line). The peak amplitude is the maximum value of the LFP power (b black line) during stimulation (c). The area under the curve (AUC) during the stimulation period (10–30 s) was compared with the pre-stimulation period (0–10 s) (d). The difference of peak amplitude and AUC shows no significance between the conditions (saline or TGN-020) ($p < 0.05$ Bonferroni correction with a paired t-test.).

https://doi.org/10.1371/journal.pone.0228759.g001
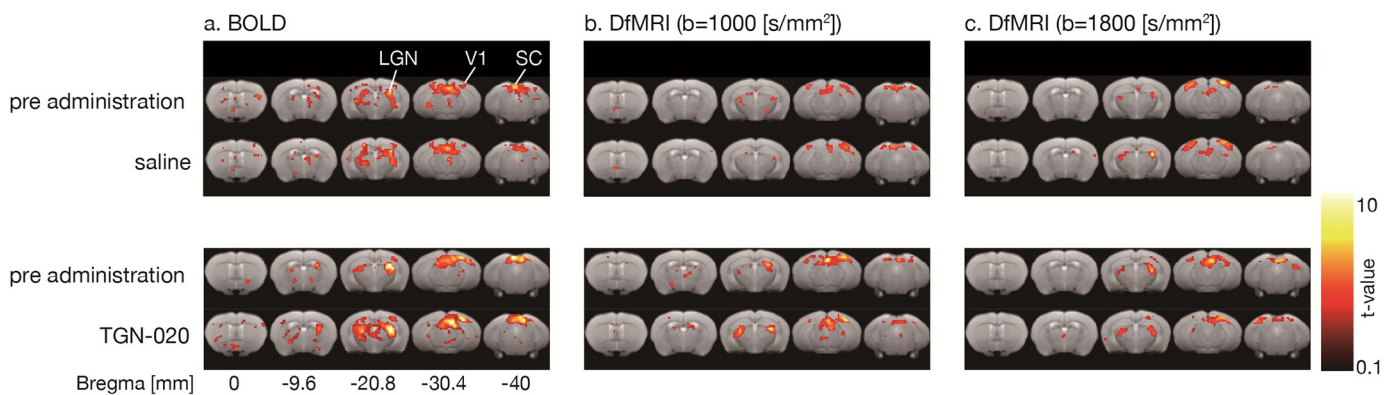
Fig 2. Activation maps (a: BOLD, b: DfMRI b1000; c: DfMRI b1800)—Comparison of activation maps before and after TGN-020 or saline administration ($p < 0.05$, FDR corrected). (a) BOLD, (b) DfMRI (b = 1000 [s/mm^2]), (c) DfMRI (b = 1800 [s/mm^2]). Activation was observed in V1, SC, LGN.

https://doi.org/10.1371/journal.pone.0228759.g002
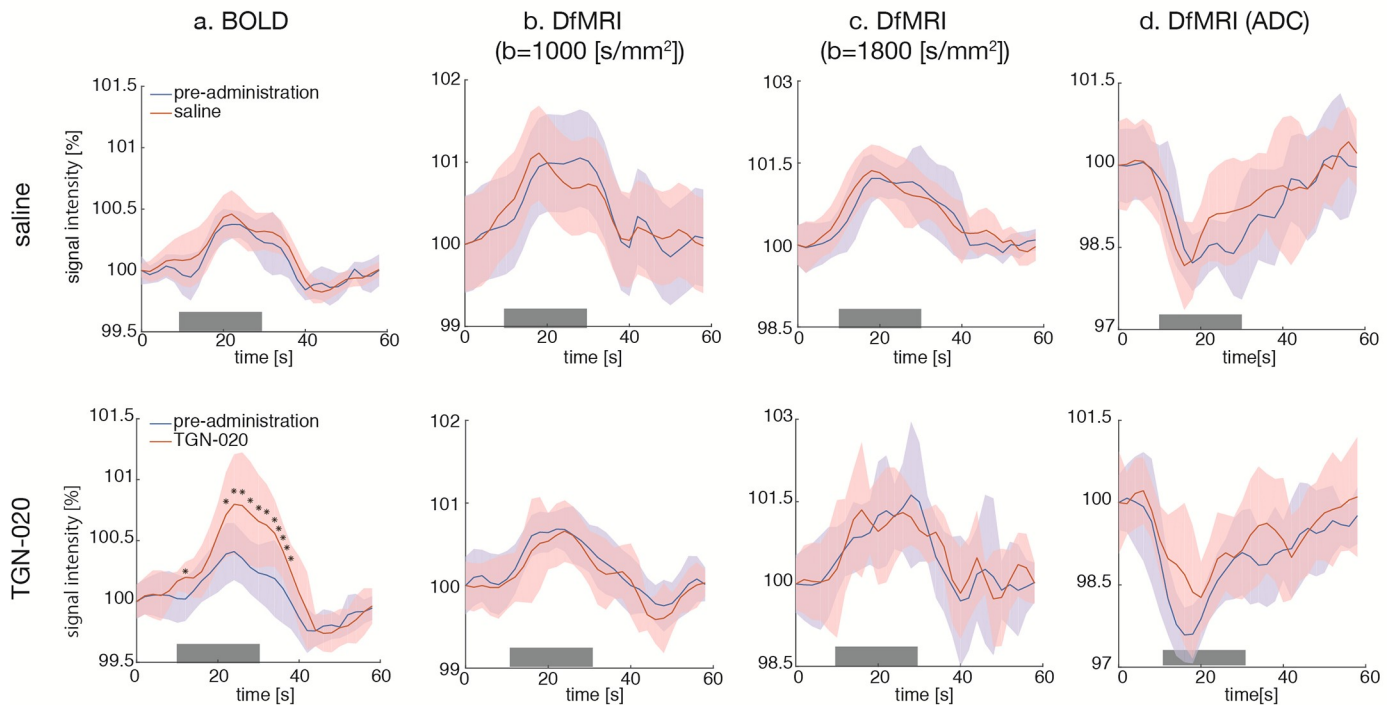
Fig 3. Time courses (a: BOLD; b: b1000; c: b1800; d: ADC)—Time courses of signal in V1 with saline (upper row) and TGN-020 (lower row). (a) BOLD, (b) DfMRI (b = 1000 [s/mm²]), (c) DfMRI (b = 1800 [s/mm²]), (d) DfMRI (ADC). The amplitude of the BOLD response after TGN-020 administration (red line) is significantly larger than the pre-administration response (blue line), while the amplitude of the DfMRI and ADC responses after TGN-020 administration are not significantly different. The color bands represent the standard deviation (SD) between subjects (n = 9). The visual stimulus was applied between 10 and 30 seconds (gray bar). An asterisk indicates a significant difference between pre-administration and post-administration (paired t-test, p<0.05). Note that the onset and offset of the DfMRI signal response occur earlier than for the BOLD fMRI responses.

https://doi.org/10.1371/journal.pone.0228759.g003

oxygen consumption and blood flow in local vessels, both of which increase during neural activation [8]. Hence, BOLD fMRI primarily reflects changes in hemodynamics and oxygenation, not directly neural activity, resulting in known limitations, namely its limited spatial and temporal resolution with regards to underlying neural activity [9, 33], its sensitivity to underlying local organizational structure of the vascular network (which may not always covariate with local neural networks [34]) and to any confound interfering with the neurovascular mechanism (underlying pathology, presence of drugs, notably anesthetic drugs) [9, 17].

To overcome the limitations of BOLD fMRI, alternative fMRI imaging methods have been previously proposed. One of them, DfMRI, monitors changes in water diffusion occurring in activated brain tissue [1]. DfMRI has been found to be more accurate in time and space than the BOLD response [5,35,36] and it is thought to be more directly reflecting neural activation status. Activation-induced cell swelling has been proposed as its hypothetical mechanism [10,11] and recent studies have shown that the DfMRI signal is not related to the neurovascular coupling [19] and that, contrarily to BOLD the DfMRI signal is modulated by neuronal swelling inhibition and cell swelling facilitation [17], mirroring LFP responses. While the likely cell population involved is neuronal (dendritic spines) contribution of astrocytes has not been ruled out.

Here we used another pharmacological challenge based on the inhibition of AQP4 channels carried specifically by astrocytes. Astrocytes are thought to play a major role in neurovascular coupling [21]. Excitatory events can drive activity in interneurons [37] or astrocytes [38,39]
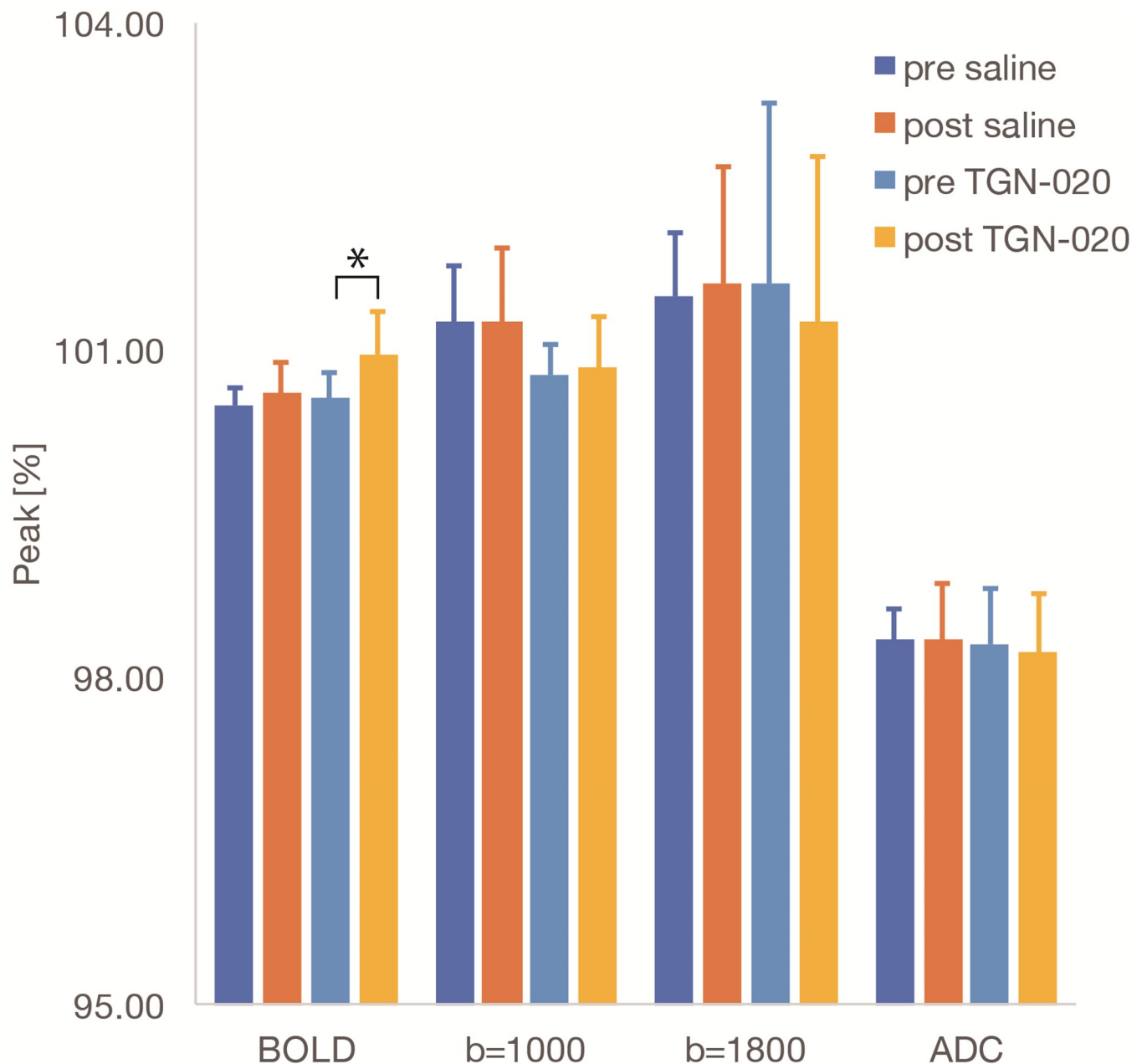
Fig 4. Bar plots for peak amplitude responses—Peak amplitude response before and after TGN-020 or saline administration. The peak amplitude of the BOLD signal change was significantly higher after TGN-020 administration, no change was observed for the DfMRI signal at b = 1000, b = 1800s/mm², and for the ADC. The error bars represent the SD between subjects (n = 9). An asterisk indicates a significant difference between pre-administration and TGN-020 administration (p<0.05, paired t-test).

that recruit a local hemodynamic response [40]. Upon neuronal activity through Ca²⁺ signaling, astrocytes release vasoactive substances which promote arteriolar vasodilatation and cause a CBF increase from the baseline [41], but the exact mechanisms are still not well understood and other studies have revealed a more complicated relationship between neuronal/glial activity and BOLD responses [25]. TGN-020 is known to increase astrocyte swelling, reduce water

flow from astrocytes into the peri-capillary Virchow-Robin space, reduce peri-capillary fluid pressure and capillary lumen expansion and increase regional baseline CBF [24,42]. Here, we found that the amplitude of the BOLD response triggered by visual stimulation was increased under TGN-020 administration. Assuming that under TGN-020 astrocyte function is disrupted by blockage of AQP4 channels [43] those results confirm the involvement of astrocytes in the neurovascular mechanisms underlying BOLD fMRI [44–47] as neuronal activity (as assessed from LFPs) remained unchanged. Indeed, LFPs have not been found altered by acute inhibition of the AQP4, although excitatory postsynaptic spiking through K^+ spatial buffering as well as NMDA-mediated excitatory postsynaptic currents, closely related to MUA, are altered in AQP4 KO mice [26,48]. LFPs integrates excitatory and inhibitory postsynaptic activity within the complex synaptic architectural organization [49]. Intraperitoneal injection of TGN-020 suppresses phosphorylated extracellular regulated protein kinase (pERK), which is a neuronal activity marker also related to cell swelling [43,50]. Inhibition of pERK expression increases reactive oxygen species (ROS) in mitochondria of astrocytes [51, 52]. Those alterations in astrocyte function might lead to a BOLD amplitude increase. However, such molecular mechanisms are very speculative and out of the scope of this work.

A potential mechanism could be an increase in baseline CBF which is known to increase under administration of TGN-020 [41,53]. Functionally induced changes in CBF are thought to be proportional to the underlying baseline CBF, resulting in constant relative changes in CBF upon activation, however some studies have suggested that activation driven changes in CBF are independent from baseline [54–56]. Administration of acetazolamide which increases CBF by vasodilation decreases the BOLD contrast under visual stimulation [57]. Those conflicting results reflect the complexity of the mechanisms involved in neurovascular coupling, which in turn influences BOLD fMRI responses. In any case it was not possible to evaluate baseline CBF from BOLD signals which are only relative and not absolute by nature. Furthermore, we cannot rule out that BOLD responses might reflect oxygen consumption activity in the astrocytes [21]. Clearly, further studies should be performed to investigate the cellular and molecular mechanisms underlying alteration of the neurovascular coupling by TGN-020.

In any case, the absence of direct effects of TGN-020 on neural activity, as evidenced from LFPs, we must conclude that the increase in BOLD fMRI responses that we observed under TGN-020 reflect changes in astrocyte activity. In contrast, the present results clearly demonstrate that DfMRI responses (acquired at high b values) and resulting ADC values are not affected by TGN-020 administration. Assuming astrocyte activity was perturbed by AQP4 inhibition through TGN-020 administration, while neural responses were not we must conclude that, contrarily to BOLD fMRI responses, DfMRI responses were not affected by astrocyte activity disruption, and that astrocytes contribution to the DfMRI responses is very small if any. Those results also confirm that DfMRI is immune to disruptions in hemodynamics and neurovascular coupling underlying BOLD fMRI, reflecting in a more robust way neural responses [17].

In this study LFPs could be recorded only in one location, V1, following visual stimulation. Recording LFPs was obviously necessary to allow interpretation of both BOLD fMRI and DfMRI responses to disentangle potential effects of TGN-020 on neural and vascular systems. However, neurovascular coupling level, astrocytes contribution and AQP4 expression might vary across brain locations. Especially, it would be interesting to compare in the future BOLD fMRI and DfMRI responses in areas located within cerebellum and hippocampus (CA1) which are rich in AQP4 receptors.

In this study, the BOLD fMRI responses were obtained from spin-echo (SE-EPI) sequences (instead of more standard gradient-echo EPI (GE-EPI) sequences). Beside convenience and reliability (the same MRI sequence was used for both BOLD fMRI and DfMRI) SE-EPI is

known to be more accurate than GE-EPI (without contamination from draining veins and large vessels) and more robust to background susceptibility artifacts. However, a drawback is that SE-EPI BOLD fMRI responses are smaller in amplitudes than with GE-EPI BOLD fMRI, so that the observed differences in BOLD fMRI and DfMRI responses amplitudes may vary when GE-EPI sequences are used.

An important point to underline is that, although the same SE-EPI MRI sequence was used, different behaviors were observed depending on the b values (degree of diffusion weighting) associated with the sequence. With b = 0 BOLD effects were solely visible. Using a high diffusion weighting (b = 1000 and 1800s/mm^2) a completely different behavior emerged as shown here. This means that the contribution of the water diffusion effect to the signal largely predominates over the contribution of T2 which remains the same whatever the b value. Residual T2 effects are, furthermore, removed when calculating the ADC which solely reflects diffusion effects. The decrease in ADC upon neural activation, as we observed, is fully consistent with earlier reports [1,3,5,17–20] and generally reflects a local increase in cell size, further confirming the neural swelling hypothesis of DfMRI mechanisms. Activation driven neural swelling should be distinguished from the astrocyte swelling which may have also occurred by blocking AQP4 channels. Such astrocyte swelling could result in a small ADC decrease, but it was not observed within the conditions of this study. Indeed, although astrocyte activity may have been altered by TGN-020 there is no indication that astrocyte swelling actually occurred. While inhibition of AQP4 channels by TGN-020 has been shown initially through oocyte swelling [22] the effects of TGN-020 on water transport have been controversial [58,59].

An alternative, more robust method would have been to investigate BOLD and DfMRI responses in AQP4 knockout or knockdown mice [60,61]. However, in contrast to acute inhibition of AQP4 by pharmacological agents, some brain features in AQP4 knockout mice are abnormal, for instance, increased cerebral capillary densities and impaired neuronal differentiation of adult neural stem cells [60,61]. Differences in BOLD and DfMRI responses would then likely reflect predominantly such alteration rather than the astrocyte activity, which would be certainly interesting to investigate.

One may rightly question why DfMRI has not yet become popular for fMRI given the limitations of BOLD fMRI. Those limitations might be acceptable for human cognitive imaging on a coarse spatiotemporal resolution but represent an important drawback for neuroscience applications at a finer level or when using preclinical models under anesthesia. The main reason for the limited usage of DfMRI is likely technical due to the relatively higher noise level observed with long TE, spin-echo based diffusion MRI compared to gradient-echo based BOLD fMRI (the amplitude of the diffusion and BOLD fMRI responses are otherwise very similar as shown in this study), which may require signal averaging over repeated fMRI sessions, a potential limitation for human studies. Another possible reason is that the putative mechanism underlying DfMRI and its direct link with neural activity (ie, neuromechanical coupling) has not yet been directly evidenced. Hopefully, this uncertainty will dissipate over time given the accumulation of studies, like this one, revealing the differential mechanisms beyond DfMRI and BOLD fMRI.

Conclusion

Disruption of astrocyte function by blocking AQP4 channels impacts BOLD fMRI responses in V1 following visual stimulation but not DfMRI responses. This discrepancy confirms that while BOLD fMRI depends on neurovascular coupling, DfMRI relies on a different mechanism not involving astrocytes.

Supporting information

S1 Fig. High-frequency spiking activity (a). The visual stimulus was applied between 10 and 30 seconds (a, blue block). High-frequency spiking activity obtained by applying a moving average filter of 0.001 s width window (a, black line). The peak amplitude corresponds to the maximum value during stimulation (b). The area under the curve (AUC) during the stimulation period (10–30 s) was compared with the pre-stimulation period (0–10 s) for all conditions (c). There was no significant difference in peak amplitude and AUC between the conditions (saline or TGN-020) ($p < 0.05$ Bonferroni correction with a paired t-test.).
(JPEG)

Author Contributions

Conceptualization: Yuji Komaki, Tomokazu Tsurugizawa, Denis Le Bihan.

Data curation: Yuji Komaki, Clement Debacker, Boucif Djemai, Tomokazu Tsurugizawa.

Formal analysis: Yuji Komaki, Tomokazu Tsurugizawa, Denis Le Bihan.

Funding acquisition: Denis Le Bihan.

Investigation: Yuji Komaki, Tomokazu Tsurugizawa, Denis Le Bihan.

Methodology: Yuji Komaki, Clement Debacker, Luisa Ciobanu, Tomokazu Tsurugizawa, Denis Le Bihan.

Resources: Denis Le Bihan.

Supervision: Luisa Ciobanu, Tomokazu Tsurugizawa, Denis Le Bihan.

Validation: Denis Le Bihan.

Visualization: Yuji Komaki.

Writing – original draft: Yuji Komaki, Tomokazu Tsurugizawa, Denis Le Bihan.

Writing – review & editing: Yuji Komaki, Clement Debacker, Luisa Ciobanu, Tomokazu Tsurugizawa, Denis Le Bihan.

References

1. Le Bihan D, Urayama S, Aso T, Hanakawa T, Fukuyama H. Direct and fast detection of neuronal activation in the human brain with diffusion MRI. Proc Natl Acad Sci U S A. 2006/05/17. 2006; 103: 8263–8268. https://doi.org/10.1073/pnas.0600644103 PMID: 16702549

2. De Luca A, Schlaffke L, Siero JCW, Froeling M, Leemans A. On the sensitivity of the diffusion MRI signal to brain activity in response to a motor cortex paradigm. Hum Brain Mapp. 2019; 40: 5069–5082. https://doi.org/10.1002/hbm.24758 PMID: 31410939

3. Aso T, Urayama S ichi, Poupon C, Sawamoto N, Fukuyama H, Le Bihan D. An intrinsic diffusion response function for analyzing diffusion functional MRI time series. Neuroimage. 2009; 47: 1487–1495. https://doi.org/10.1016/j.neuroimage.2009.05.027 PMID: 19450693

4. Albers F, Wachsmuth L, Schache D, Lambers H, Faber C. Functional mri readouts from bold and diffusion measurements differentially respond to optogenetic activation and tissue heating. Front Neurosci. 2019; 13: 1–16.

5. Nunes D, Ianus A, Shemesh N. Layer-specific connectivity revealed by diffusion-weighted functional MRI in the rat thalamocortical pathway. Neuroimage. 2019; 184: 646–657. https://doi.org/10.1016/j.neuroimage.2018.09.050 PMID: 30267858

6. Miller KL, Bulte DP, Devlin H, Robson MD, Wise RG, Woolrich MW, et al. Evidence for a vascular contribution to diffusion FMRI at high b value. Proc Natl Acad Sci U S A. 2007; 104: 20967–20972. https://doi.org/10.1073/pnas.0707257105 PMID: 18093924

7. Bai R, Stewart CV, Plenz D, Basser PJ. Assessing the sensitivity of diffusion MRI to detect neuronal activity directly. Proc Natl Acad Sci U S A. 2016; 113: E1728–37. https://doi.org/10.1073/pnas.1519890113 PMID: 26941239

8. Ogawa S, Lee TM, Kay AR, Tank DW. Brain magnetic resonance imaging with contrast dependent on blood oxygenation. Proc Natl Acad Sci U S A. 1990; 87: 9868–72. https://doi.org/10.1073/pnas.87.24.9868 PMID: 2124706

9. Schmithorst VJ, Vannest J, Lee G, Hernandez-Garcia L, Plante E, Rajagopal A, et al. Evidence that neurovascular coupling underlying the BOLD effect increases with age during childhood. Hum Brain Mapp. 2015; 36: 1–15. https://doi.org/10.1002/hbm.22608 PMID: 25137219

10. Andrew RD, MacVicar BA. Imaging cell volume changes and neuronal excitation in the hippocampal slice. Neuroscience. 1994; 62: 371–383. https://doi.org/10.1016/0306-4522(94)90372-7 PMID: 7830884

11. Cohen LB, Keynes RD, Hille B. Light scattering and birefringence changes during nerve activity. Nature. 1968; 218: 438–441. https://doi.org/10.1038/218438a0 PMID: 5649693

12. Sotak CH. Nuclear magnetic resonance (NMR) measurement of the apparent diffusion coefficient (ADC) of tissue water and its relationship to cell volume changes in pathological states. Neurochem Int. 2004; 45: 569–582. https://doi.org/10.1016/j.neuint.2003.11.010 PMID: 15186924

13. van der Toorn A, Sykova E, Dijkhuizen RM, Vorisek I, Vargova L, Skobisova E, et al. Dynamic changes in water ADC, energy metabolism, extracellular space volume, and tortuosity in neonatal rat brain during global ischemia. Magn Reson Med. 1996; 36: 52–60. https://doi.org/10.1002/mrm.1910360110 PMID: 8795020

14. O'Shea JM, Williams SR, van Bruggen N, Gardner-Medwin AR. Apparent diffusion coefficient and MR relaxation during osmotic manipulation in isolated turtle cerebellum. Magn Reson Med. 2000; 44: 427–432. https://doi.org/10.1002/1522-2594(200009)44:3<427::aid-mrm13>3.0.co;2-b PMID: 10975895

15. Buckley DL, Bui JD, Phillips MI, Zelles T, Inglis BA, Plant HD, et al. The effect of ouabain on water diffusion in the rat hippocampal slice measured by high resolution NMR imaging. Magn Reson Med. 1999; 41: 137–142. https://doi.org/10.1002/(sici)1522-2594(199901)41:1<137::aid-mrm19>3.0.co;2-y PMID: 10025621

16. Le Bihan D. Diffusion MRI: what water tells us about the brain. EMBO Mol Med. 2014; 6: 569–573. https://doi.org/10.1002/emmm.201404055 PMID: 24705876

17. Abe Y, Tsurugizawa T, Le Bihan D. Water diffusion closely reveals neural activity status in rat brain loci affected by anesthesia. PLoS Biol. 2017; 15: 1–24. https://doi.org/10.1371/journal.pbio.2001494 PMID: 28406906

18. Abe Y, Van Nguyen K, Tsurugizawa T, Ciobanu L, Le Bihan D. Modulation of water diffusion by activation-induced neural cell swelling in Aplysia Californica. Sci Rep. 2017; 7: 1–8.

19. Tsurugizawa T, Ciobanu L, Le Bihan D. Water diffusion in brain cortex closely tracks underlying neuronal activity. Proc Natl Acad Sci. 2013. https://doi.org/10.1073/pnas.1303178110 PMID: 23801756

20. Tsurugizawa T, Abe Y, Le Bihan D. Water apparent diffusion coefficient correlates with gamma oscillation of local field potentials in the rat brain nucleus accumbens following alcohol injection. J Cereb Blood Flow Metab. 2017; 37: 3193–3202. https://doi.org/10.1177/0271678X16685104 PMID: 28058981

21. Takata N, Sugiura Y, Yoshida K, Koizumi M, Hiroshi N, Honda K, et al. Optogenetic astrocyte activation evokes BOLD fMRI response with oxygen consumption without neuronal activity modulation. Glia. 2018; 66: 2013–2023. https://doi.org/10.1002/glia.23454 PMID: 29845643

22. Huber VJ, Tsujita M, Nakada T. Identification of Aquaporin 4 inhibitors using in vitro and in silico methods. Bioorganic Med Chem. 2009; 17: 411–417. https://doi.org/10.1016/j.bmc.2007.12.040 PMID: 18182301

23. Amiry-Moghaddam M, Otsuka T, Hurn PD, Traystman RJ, Haug F-M, Froehner SC, et al. An -syntrophin-dependent pool of AQP4 in astroglial end-feet confers bidirectional water flow between blood and brain. Proc Natl Acad Sci. 2003; 100: 2106–2111. https://doi.org/10.1073/pnas.0437946100 PMID: 12578959

24. Igarashi H, Tsujita M, Suzuki Y, Kwee IL, Nakada T. Inhibition of aquaporin-4 significantly increases regional cerebral blood flow. Neuroreport. 2013; 24: 324–328. https://doi.org/10.1097/WNR.0b013e32835fc827 PMID: 23462267

25. Iadecola C. Neurovascular regulation in the normal brain and in Alzheimer's disease. Nat Rev Neurosci. 2004; 5: 347–360. https://doi.org/10.1038/nrn1387 PMID: 15100718

26. Goense JBM, Logothetis NK. Neurophysiology of the BOLD fMRI signal in awake monkeys. Curr Biol. 2008; 18: 631–640. https://doi.org/10.1016/j.cub.2008.03.054 PMID: 18439825

27. Komaki Y, Hikishima K, Shibata S, Konomi T, Seki F, Yamada M, et al. Functional brain mapping using specific sensory-circuit stimulation and a theoretical graph network analysis in mice with neuropathic allodynia. Sci Rep. 2016; 6: 37802. https://doi.org/10.1038/srep37802 PMID: 27898057

28. Oh SW, Harris JA, Ng L, Winslow B, Cain N, Mihalas S, et al. A mesoscale connectome of the mouse brain. Nature. 2014; 508: 207–214. https://doi.org/10.1038/nature13186 PMID: 24695228

29. Lein ES, Hawrylycz MJ, Ao N, Ayres M, Bensinger A, Bernard A, et al. Genome-wide atlas of gene expression in the adult mouse brain. Nature. 2007; 445: 168–176. https://doi.org/10.1038/nature05453 PMID: 17151600

30. Xing D, Yeh C-I, Shapley RM. Spatial Spread of the Local Field Potential and its Laminar Variation in Visual Cortex. J Neurosci. 2009; 29: 11540–11549. https://doi.org/10.1523/JNEUROSCI.2573-09.2009 PMID: 19759301

31. Burns SP, Xing D, Shapley RM. Comparisons of the dynamics of local field potential and multiunit activity signals in macaque visual cortex. J Neurosci. 2010; 30: 13739–13749. https://doi.org/10.1523/JNEUROSCI.0743-10.2010 PMID: 20943914

32. Pauling L, Coryell CD. The Magnetic Properties and Structure of Hemoglobin, Oxyhemoglobin and Carbonmonoxyhemoglobin. Proc Natl Acad Sci. 1936; 22: 210–216. https://doi.org/10.1073/pnas.22.4.210 PMID: 16577697

33. O'Herron P, Chhatbar PY, Levy M, Shen Z, Schramm AE, Lu Z, et al. Neural correlates of single-vessel haemodynamic responses in vivo. Nature. 2016; 534: 378–382. https://doi.org/10.1038/nature17965 PMID: 27281215

34. Boido D, Rungta RL, Osmanski B-F, Roche M, Tsurugizawa T, Le Bihan D, et al. Mesoscopic and microscopic imaging of sensory responses in the same animal. Nat Commun. 2019; 10: 1110. https://doi.org/10.1038/s41467-019-09082-4 PMID: 30846689

35. Nicolas R, Gros-Dagnac H, Aubry F, Celsis P. Comparison of BOLD, diffusion-weighted fMRI and ADC-fMRI for stimulation of the primary visual system with a block paradigm. Magn Reson Imaging. 2017; 39: 123–131. https://doi.org/10.1016/j.mri.2017.01.022 PMID: 28163122

36. Williams RJ, Reutens DC, Hocking J. Functional localization of the human color center by decreased water displacement using diffusion-weighted fMRI. Brain Behav. 2015; 5: 1–12.

37. Cauli B, Tong XK, Rancillac A, Serluca N, Lambolez B, Rossier J, et al. Cortical GABA interneurons in neurovascular coupling: Relays for subcortical vasoactive pathways. J Neurosci. 2004; 24: 8940–8949. https://doi.org/10.1523/JNEUROSCI.3065-04.2004 PMID: 15483113

38. Haydon PG, Carmignoto G. Astrocyte control of synaptic transmission and neurovascular coupling. Physiol Rev. 2006; 86: 1009–1031. https://doi.org/10.1152/physrev.00049.2005 PMID: 16816144

39. Mulligan SJ, MacVicar BA. Calcium transients in astrocyte endfeet cause cerebrovascular constrictions. Nature. 2004; 431: 195–199. https://doi.org/10.1038/nature02827 PMID: 15356633

40. Zonta M, Angulo MC, Gobbo S, Rosengarten B, Hossmann KA, Pozzan T, et al. Neuron-to-astrocyte signaling is central to the dynamic control of brain microcirculation. Nat Neurosci. 2003; 6: 43–50. https://doi.org/10.1038/nn980 PMID: 12469126

41. Girouard H, Iadecola C. Neurovascular coupling in the normal brain and in hypertension, stroke, and Alzheimer disease. J Appl Physiol. 2005; 100: 328–335. https://doi.org/10.1152/japplphysiol.00966.2005 PMID: 16357086

42. Nakada T, Kwee IL, Igarashi H, Suzuki Y. Aquaporin-4 functionality and virchow-robin space water dynamics: Physiological model for neurovascular coupling and glymphatic flow. Int J Mol Sci. 2017; 18. https://doi.org/10.3390/ijms18081798 PMID: 28820467

43. Zhao L, Li D, Liu N, Liu L, Zhang Z, Gao C, et al. Correlation of TGN-020 with the analgesic effects via ERK pathway activation after chronic constriction injury. Mol Pain. 2018; 14: 1744806918796057. https://doi.org/10.1177/1744806918796057 PMID: 30152258

44. Petzold GC, Murthy VN. Role of Astrocytes in Neurovascular Coupling. Neuron. 2011; 71: 782–797. https://doi.org/10.1016/j.neuron.2011.08.009 PMID: 21903073

45. Jolivet R, Coggan JS, Allaman I, Magistretti PJ. Multi-timescale Modeling of Activity-Dependent Metabolic Coupling in the Neuron-Glia-Vasculature Ensemble. PLoS Comput Biol. 2015; 11: 1–23. https://doi.org/10.1371/journal.pcbi.1004036 PMID: 25719367

46. Du W, Iddings JA, Morrison HW, Kim KJ, Filosa JA. Beyond neurovascular coupling, role of astrocytes in the regulation of vascular tone. Neuroscience. 2015; 323: 96–109. https://doi.org/10.1016/j.neuroscience.2015.03.064 PMID: 25843438

47. Drake CT, Iadecola C. The role of neuronal signaling in controlling cerebral blood flow. Brain Lang. 2007; 102: 141–152. https://doi.org/10.1016/j.bandl.2006.08.002 PMID: 17010421

48. Li YK, Wang F, Wang W, Luo Y, Wu PF, Xiao JL, et al. Aquaporin-4 deficiency impairs synaptic plasticity and associative fear memory in the lateral amygdala: Involvement of downregulation of glutamate transporter-1 expression. Neuropsychopharmacology. 2012; 37: 1867–1878. https://doi.org/10.1038/npp.2012.34 PMID: 22473056

49. Buzsaki G, Anastassiou CA, Koch C. The origin of extracellular fields and currents—EEG, ECoG, LFP and spikes. Nat Rev Neurosci. 2012; 13: 407–420. https://doi.org/10.1038/nrn3241 PMID: 22595786

50. Qi L-L, Fang S-H, Shi W-Z, Huang X-Q, Zhang X-Y, Lu Y-B, et al. CysLT2 receptor-mediated AQP4 up-regulation is involved in ischemic-like injury through activation of ERK and p38 MAPK in rat astrocytes. Life Sci. 2011; 88: 50–56. https://doi.org/10.1016/j.lfs.2010.10.025 PMID: 21055410

51. Cesi G, Walbrecq G, Zimmer A, Kreis S, Haan C. ROS production induced by BRAF inhibitor treatment rewires metabolic processes affecting cell growth of melanoma cells. Mol Cancer. 2017; 16: 102. https://doi.org/10.1186/s12943-017-0667-y PMID: 28595656

52. Park L, Anrather J, Girouard H, Zhou P, Iadecola C. Nox2-derived reactive oxygen species mediate neurovascular dysregulation in the aging mouse brain. J Cereb Blood Flow Metab. 2007; 27(12):1908–18. https://doi.org/10.1038/sj.jcbfm.9600491 PMID: 17429347

53. Igarashi H, Huber VJ, Tsujita M, Nakada T. Pretreatment with a novel aquaporin 4 inhibitor, TGN-020, significantly reduces ischemic cerebral edema. Neurol Sci. 2011; 32: 113–116. https://doi.org/10.1007/s10072-010-0431-1 PMID: 20924629

54. Kemna LJ, Posse S. Effect of respiratory CO2changes on the temporal dynamics of the hemodynamic response in functional MR imaging. Neuroimage. 2001; 14: 642–649. https://doi.org/10.1006/nimg.2001.0859 PMID: 11506537

55. Cohen ER, Ugurbil K, Kim S. Effect of Basal Conditions on the Magnitude and Dynamics of the Hemodynamic Response. Mind. 2002; 10: 57180–57180.

56. Shimosegawa E, Hatazawa J, Fujita H, Okudera T, Kanno I, Ogawa T, et al. Photic Stimulation Study of Changing the Arterial Partial Pressure Level of Carbon Dioxide. J Cereb Blood Flow Metab. 2011; 15: 111–114. https://doi.org/10.1038/jcbfm.1995.12 PMID: 7798327

57. Hänicke W, Frahm J, Merboldt K-D, Kleinschmidt A, Bruhn H, Boecker H. The Effect of Acetazolamide on Regional Cerebral Blood Oxygenation at Rest and under Stimulation as Assessed by MRI. J Cereb Blood Flow Metab. 2011; 14: 742–748. https://doi.org/10.1038/jcbfm.1994.95 PMID: 8063870

58. Tradtrantip L, Jin B-J, Yao X, Anderson MO, Verkman AS. Aquaporin-Targeted Therapeutics: State-of-the-Field. Adv Exp Med Biol. 2017; 969: 239–250. https://doi.org/10.1007/978-94-024-1057-0_16 PMID: 28258578

59. Yang B, Zhang H, Verkman AS. Lack of aquaporin-4 water transport inhibition by antiepileptics and aryl-sulfonamides. Bioorg Med Chem. 2008; 16: 7489–7493. https://doi.org/10.1016/j.bmc.2008.06.005 PMID: 18572411

60. Badaut J, Ashwal S, Adami A, Tone B, Recker R, Spagnoli D, et al. Brain water mobility decreases after astrocytic aquaporin-4 inhibition using RNA interference. J Cereb Blood Flow Metab. 2011; 31: 819–831. https://doi.org/10.1038/jcbfm.2010.163 PMID: 20877385

61. Manley GT, Fujimura M, Ma T, Noshita N, Filiz F, Bollen AW, et al. Aquaporin-4 deletion in mice reduces brain edema after acute water intoxication and ischemic stroke. Nat Med. 2000; 6: 159–163. https://doi.org/10.1038/72256 PMID: 10655103